ACADEMIC PRESS

Available online at www.sciencedirect.com
SCIENCE DIRECT®

NeuroImage

NeuroImage 20 (2003) 1064–1075

www.elsevier.com/locate/ynimg

Mapping of brain function after MPTP-induced neurotoxicity in a primate Parkinson's disease model

Anna-Liisa Brownell,[a,d,*] Kelly Canales,[a] Y. Iris Chen,[a] Bruce G. Jenkins,[a] Christopher Owen,[b] Elijahu Livni,[a] Meixiang Yu,[a] Francesca Cicchetti,[d] Rosario Sanchez-Pernaute,[c] and Ole Isacson[c,d]

[a] *Department of Radiology, Massachusetts General Hospital, Boston, MA 02114, USA*
[b] *Department of Neurosurgery, Massachusetts General Hospital, Boston, MA 02114, USA*
[c] *Department of Neurology, Massachusetts General Hospital, Boston, MA 02114, USA*
[d] *Udall Parkinson's Disease Research Center of Excellence, Neuroregeneration Laboratory, McLean Hospital, Belmont, MA 02478, USA*

Received 30 October 2002; revised 1 June 2003; accepted 3 June 2003

Abstract

Neurophysiological studies of the brain in normal and Parkinson's disease (PD) patients have indicated intricate connections for basal ganglia-induced control of signaling into the motor cortex. To investigate if similar mechanisms are controlling function in the primate brain (*Macaca fascicularis*) after MPTP-induced neurotoxicity, we conducted PET studies of cerebral blood flow, oxygen and glucose metabolism, dopamine transporter, and D2 receptor function. Our observations after MPTP-induced dopamine terminal degeneration of the caudate and putamen revealed increased blood flow (15%) in the globus pallidus (GP), while blood flow was moderately decreased (15–25%) in the caudate, putamen, and thalamus and 40 % in the primary motor cortex (PMC). Oxygen extraction fraction was moderately increased (10–20%) in other brain areas but the thalamus, where no change was observable. Oxygen metabolism was increased in the GP and SMA (supplementary motor area including premotor cortex, Fig. 3) by a range of 20–40% and decreased in the putamen and caudate and in the PMC. Glucose metabolism was decreased in the caudate, putamen, thalamus, and PMC (range 35–50%) and enhanced in the GP by 15%. No change was observed in the SMA. In the parkinsonian primate, [^{11}C]CFT (2β-carbomethoxy-3β-(4-fluorophenyltropane) dopamine transporter binding was significantly decreased in the putamen and caudate (range 60–65%). [^{11}C]Raclopride binding of dopamine D_2 receptors did not show any significant changes. These experimental results obtained in primate studies of striato-thalamo-cortico circuitry show a similar trend as hypothetized in Parkinson's disease-type degeneration.

Keywords: Positron emission tomography; Volume rendering; MPTP; Parkinson's disease

Introduction

Parkinson's disease (PD) is characterized neuropathologically by a severe depletion of DA neurons and an associated loss of axons and terminals in the basal ganglia (Kish et al., 1988). Diagnosis is based on clinical signs of tremor, rigidity, bradykinesia, and postural instability (Marsden, 1992).

Hypotheses of the etiology of PD focus on the potential contribution of environmental toxins (exogenous and/or endogenous) and their interactions with genetic components (Checkoway and Nelson, 1999; Gorrell et al., 1996; Mizuno et al., 1999; Schapira, 1996). Cell death introduced by toxins may trigger a cascade of biological processes with an endpoint of continuous degeneration (Brownell et al., 1998, 1999; Schmidt and Ferger, 2001). These biological processes affect primarily the dopaminergic system in the basal ganglia and the neural network of the motor system (Alex-

* Corresponding author. Department of Radiology, Massachusetts General Hospital, Bartlett Hall 504R, Boston, MA 02114. Fax: +1-617-726-5123.
E-mail address: abrownell@partners.org (A.L. Brownell).

1053-8119/$ – see front matter © 2003 Elsevier Inc. All rights reserved.
doi:10.1016/S1053-8119(03)00348-3

ander et al., 1986, 1990; Wichman and DeLong, 1996; DeLong and Wichman, 2001).

MPTP (1-methyl-4-phenyl-1,2,5,6-tetrahydropyridine) neurotoxicity has long been used as a model for Parkinson's disease because it induces dopaminergic cell death in the substantia nigra pars compacta and striatal dopaminergic degeneration (Palombo et al., 1991; Schmidt and Ferger, 2001). MPTP-induced dopaminergic degeneration causes decreases in the binding of presynaptic dopamine transporters and reduces locomotor activity (Hantraye et al., 1992; Wullner et al., 1994).

A number of in vivo imaging studies in PD patients have shown regional differences in glucose metabolism and blood flow (Brooks, 2001; Eidelberg et al., 1995b; Fukuda et al., 2001; Markus et al., 1995). These studies show that glucose utilization and cerebral blood flow reductions in the brain correlate with the severity of the disease (Berding et al., 2001; Eberling et al., 1994; Eidelberg et al., 1995a; Moeller and Eidelberg, 1997; Imon et al., 1999). Antonini et al. (1998) have even proposed that studies of glucose metabolism can be used for differential diagnosis of PD.

There is, however, great variability in the reports of absolute values of local metabolic functions (Antonini et al., 1995; Bohnen et al., 1999; Eberling et al., 1994). This may originate from methodological differences during imaging studies, variability in the resolution of the imaging devices and, finally, differences in the selection of regions of interest, as well as level of degenerative process. Eidelberg et al. (1996) and Brooks (2001) have used a statistical parametric mapping technique with normalized values to evaluate metabolic changes in different brain areas in PD patients before and after therapeutic regimen. Autoradiographic studies in awake primates (Palombo et al., 1990; Porrino et al., 1987) have shown significant local changes in glucose utilization in basal ganglia, cerebral cortex, and cerebellum after an unilateral intracarotid administration of MPTP.

Based on neurophysiological experiments five different loops have been characterized to control signaling between the basal ganglia and the cortex (Alexander et al., 1990). In PD, the most sensitive loop is between the putamen, globus pallidus, thalamus, and cortex. The motor loop links the supplementary motor area (SMA) to the primary motor cortex, dorsal putamen, pallidum and ventrolateral thalamus, while the dorsolateral prefrontal cortex loop links dorsal caudate and ventroanterior thalamus (Isacson et al., 2001). Studies in PD patients have postulated that the nigrostriatal DA deficiency leads to decreased inhibition of the internal segment of the globus pallidus by both direct and indirect pathways (Alexander et al., 1990). The resulting excessive inhibitory output from the globus pallidus suppresses the ventral thalamus, reducing activation of the supplementary motor area and prefrontal cortex, and creates the motor impairments characteristic of PD (Alexander, 1987; Crutcher and DeLong, 1984; Wichman and DeLong, 1996).

To investigate if similar neural circuitry-linked mechanisms are operating in primate models of parkinsonism induced by MPTP, we conducted experimental imaging studies before and after MPTP of cerebral blood flow, oxygen extraction fraction, oxygen and glucose metabolism, dopamine transporters, and dopamine D_2 receptors using positron emission tomography (PET).

For data analyses, a volumetric technique was developed to select regions of interest based both on a primate brain atlas (Paxinos et al., 2000) and on actual MRI data. PET data were coregistered with the complete brain volume of MR data, and the resulting volumetric-PET data were used for quantitative data analyses.

Methods

Procedures in primates

Five male aged monkeys (*Macaca fascicularis*) (age: 11–16 years) were injected with MPTP (0.3 or 0.5 mg/kg iv weekly) until PD symptoms appeared including hypokinesia, tremor, rigidity, and bradykinesia (Wullner et al., 1994). The total dose of the injected MPTP varied between 25 and 42 mg and the total administration time between 6 and 21 months. PET imaging studies were conducted before MPTP administrations and 2–3 months after cessation of MPTP, when the PD symptoms were stabilized. For the imaging studies, primates were anesthetized using halothane (1.5% with oxygen flow rate of 3 L/min). Arterial and venous catheterization was done for drawing blood samples and injecting of labeled ligands. Animals were adjusted into a stereotactic head holder with ear bars at the origin. Interior orbital supports ensure that images are acquired on a pseudocoronal plane perpendicular to the orbito-meatal line. This allows superposition of the data from MRI studies. Level of anesthesia, blood gases, heartbeat, and vital signs were monitored throughout the imaging procedures (Propaq, Vital Signs Monitor, Protocol Systems. Inc., Beaverton, OR).

Imaging studies of blood flow and oxygen and glucose metabolism were conducted in one imaging session, and studies of dopamine transporters and D_2 receptors were conducted in another session within the time span of a week. The MRI studies, needed for anatomical data, were conducted within a month. This short time span is necessary to eliminate possible errors in volumetric data fusion, raised by neurotoxicity-induced morphologic volumetric changes. MPTP-induced changes in blood flow, oxygen, and glucose metabolism were conducted in four primates and changes in dopamine transporter and receptor function in five primates, correspondingly.

Animals used in this study were maintained according to the guidelines of the Committee on Animals of the Harvard Medical School and Massachusetts General Hospital and of the *Guide for Care and Use of Laboratory Animals* of the Institute of the Laboratory Animal Resources, National Re-

search Council, Department of Health, Education and Welfare, Publication No. (NIH)85-23.

Detection of locomotor activity

Spontaneous locomotor activity was monitored by an Actiwatch system (Mini Mitter Company, Inc., Sunriver, OR) mounted in a shirt pocket in the back of the animal (Puyau et al., 2002). The Actiwatch reader was connected to a computer, and data were transferred from the Actiwatch to a computer through a wireless link. The Actiwatch allows analyses of circadian rhythms, average activity during light and dark, mean activity score, movement, and movement-type index. Prior to MPTP injections, there was a significant difference between day and night time locomotor activities, while after MPTP no activity difference was observable (Fig. 1). Even though the Actiwatch data cannot be used to measure clinical score of PD, it provides a useful follow-up method to visualize daily changes in spontaneous locomotor activity.

MR imaging

MR imaging was conducted in anesthetized primates using the same stereotactic head frame as in the PET studies. T2-weighted images (TR = 4500, TE = 100/10 ms) were acquired with a GE Signa 3.0 T imager in coronal planes using continuous acquisition of 3-mm slices to obtain anatomical information to be used in fusion with PET data to obtain volume of interest for quantitative analyses.

PET imaging

PET imaging studies were conducted with an in-house-built single ring PET device, PCR-I (Brownell et al., 1989). The resolution of PCR-I for a point source at the center is 4.5 mm, and the sensitivity is 46 kHz/μCi for a source of 20 cm in diameter with a concentration of 1 μCi/ml. The overall efficiency is 64% of the theoretical maximum for a 1-cm-plane thickness corresponding to the 2-cm-high detectors. The plane thickness of 5 mm used in this study is obtained by the use of cylindrical collimators, which limit the effective height of the detectors. The resolving time of PCR-I is 6 ns (FWHM). Data acquisition over the whole brain volume with this single ring device was done with 5-mm steps starting from the cerebellar level. Imaging data were corrected for uniformity, sensitivity, attenuation, decay, and acquisition time. PET images were reconstructed using a Hanning filtered convolution backprojection with a cutoff value of 1.0 (Chesler, 1973). Calibration of the positron tomograph was performed prior to each study using a cylindrical plastic phantom (diameter 6 cm) containing water solution of ^{18}F. The corrected reconstructed data set was repacked on the Linux workstation and converted into ANALYZE/AVW image format. The voxel size in coronal PET images is 5 mm in the axial Z direction and 1.19 mm $\times$ 1.19 mm in x-y plane.

After that T2-weighted MRI data from the same subject were loaded and converted into ANALYZE/AVW image format. A segmentation routine in ANALYZE was used to separate the brain from the surrounding tissue in the MRI data. PET data were then thresholded and coregistered to its respective MRI data using the NMI (Normalized Mutual Information) voxel match algorithm of the ANALYZE software package and cubic spline interpolation. A resulting transformation matrix maps the PET images onto its respective MR images, and the multimodality image registration routine returns fused PET-MRI images. The fused PET-MR images were then volume rendered for display (Fig. 2).

Selection of the volume of interest

Three-dimensional regions of interest were outlined on coronal MR slices based on anatomical borderlines observed from the primate brain atlas and MR images (Fig. 3). These regions were also computationally compared and verified with the corresponding slices in the primate brain atlas (Paxinos et al., 2000). The transformation matrix for fusing the PET data to the MRI data was then reapplied to the PET images to generate the data for three- dimensional VOI (volume of interest) analysis. Volumetric radioactivity concentration was calculated for each VOI, and these data were then used for further data analyses to calculate values for blood flow, oxygen extraction fraction and metabolism, glucose metabolism, and binding potential for dopamine transporters and dopamine D_2 receptors.

Validation of the volumetric data analyses

To validate the three-dimensional data analyses we conducted studies with a phantom consisting of two concentric spheres (Data Spectrum Corporation, Chapel Hill, NC). The volume of the inner sphere was 20 ml, and the volume of the outer sphere was 79 ml. In the first experiment the outer sphere was filled with ^{18}F-labeled water, and the inner sphere was filled with water without radioactivity. The phantom was scanned stepwise with 5-mm steps (Fig. 4). In the second experiment the inner sphere was filled with higher radioactivity concentration than in the outer sphere, which had the same radioactivity concentration as in the first experiment. Additionally, T2-weighted MR images were done with both concentric spheres filled with water. The data analyses were conducted in the same way as above by drawing ROIs on MR images and then fusing PET data with MRI data. Finally, radioactivity concentration was determined and compared with actual measured radioactivity. For comparison, radioactivity concentration was also calculated based on conventional 2-dimensional pixel analyses (Table 1).

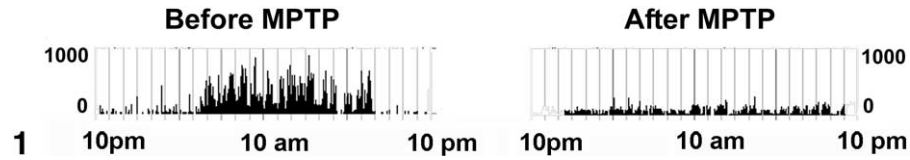

1

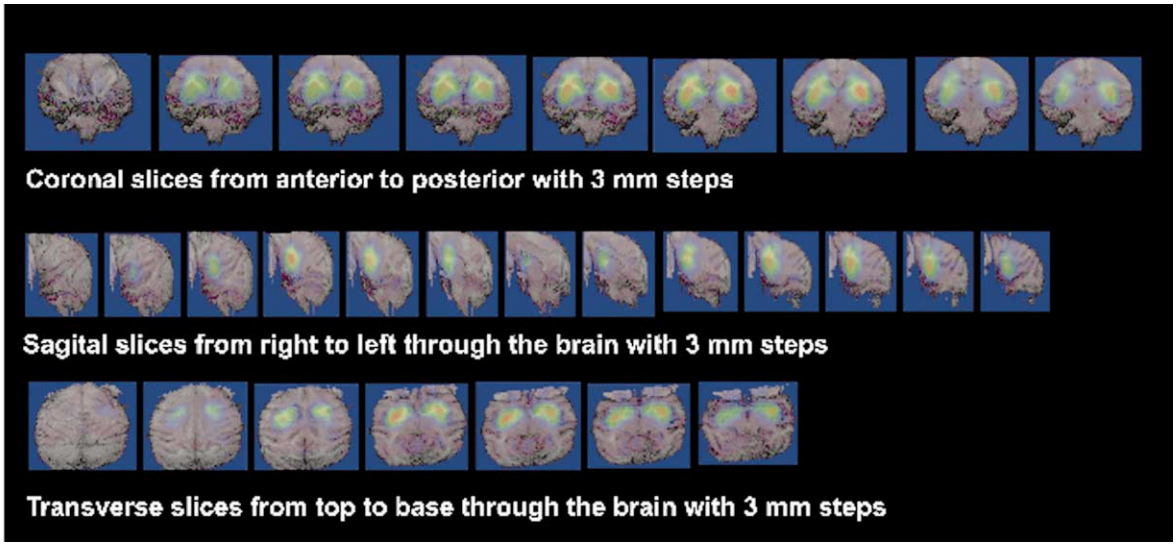

2

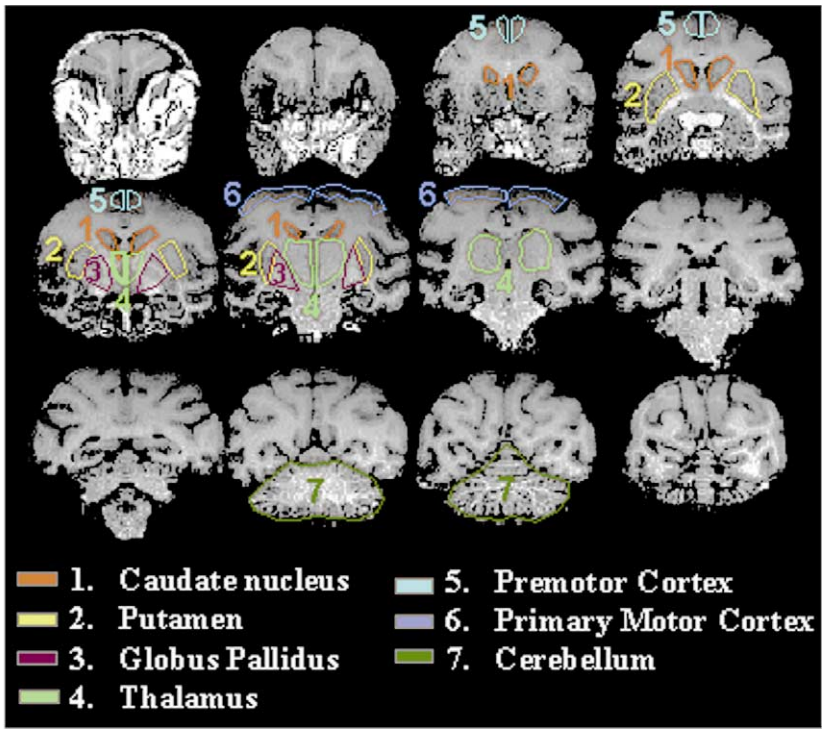

3

Fig. 1. Effect of MPTP-induced neurotoxicity on spontaneous locomotor activity detected by an Actiwatch before and after MPTP. Before MPTP there was a significant difference between day and night time locomotor activity, while after MPTP no activity difference was observable.

Fig. 2. A PET study of the distribution of [^{11}C]raclopride binding in dopamine D_2 receptors after MPTP toxicity in a primate brain. PET data were fused with volume-rendered MR images. The upper row shows coronal slices from anterior to posterior direction. Binding to D_2 receptors are localized mainly in the putamen and caudate. The middle row shows sagital slices from right to left. Slices 1–7 represent right hemisphere and slices 8–13 left hemisphere. At the bottom row transverse slices are shown from top to base. Volumetric distribution of radioactivity is used in selecting region (volumes) for interest used in quantitative data analyses of receptor function.

Fig. 3. Anatomical borderlines observed from MR images were used to define the regions of interest for volumetric data analysis on the fused PET-MRI data set. Segmented brain areas are numbered and color-coded as shown in the image. The data from the left and right hemispheres were analyzed separately.

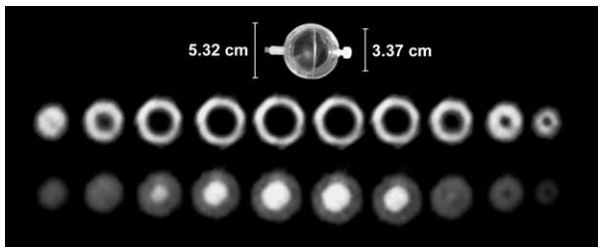

Fig. 4. To evaluate the accuracy of the volumetric data reconstruction a phantom consisting of two concentric spheres was imaged by PET. Coronal PET images were acquired with 5-mm steps and slice thickness of 5 mm over the phantom. The middle row shows images, when the outer sphere was filled with ^{18}F-labeled water and the inner sphere with water without radioactivity. The lower row shows images, when the inner sphere was filled with the same radioactivity concentration as above and activity concentration in the outer shell was about 44% of it. For data analysis PET images were fused with T2-weighted MR images and radioactivity concentrations in the inner and outer shell were determined (Table 1) using the same volumetric data analysis as in the experimental primate studies.

Blood flow studies

Blood flow studies were conducted using a steady-state technique based on the inhalation of $C^{15}O_2$ (Frackowiak et al., 1980; Jones et al., 1976; Subramanyam et al., 1978). ^{15}O-labeled CO_2 gas mixture was delivered at a constant concentration and flow rate (2 L/min) into the inhalation tube. After 6–8 min of inhalation of $C^{15}O_2$ gas mixture, a steady-state activity level was obtained in the brain, and sequential imaging over the brain was performed starting from the cerebellar level using 5-mm steps and an acquisition time of 60 s. During imaging, a series of arterial blood samples were drawn to determine blood gases and radioactivity in the plasma and whole blood. These data are needed for calculation of the oxygen extraction level (Subramanyam et al., 1978). Radioactivity was measured in a gammacounter (Packard Cobra Auto-gamma, Downers, IL), which was cross-calibrated with the tomograph. Arterial blood and plasma radioactivity concentrations were then computed after corrections for dead time and decay.

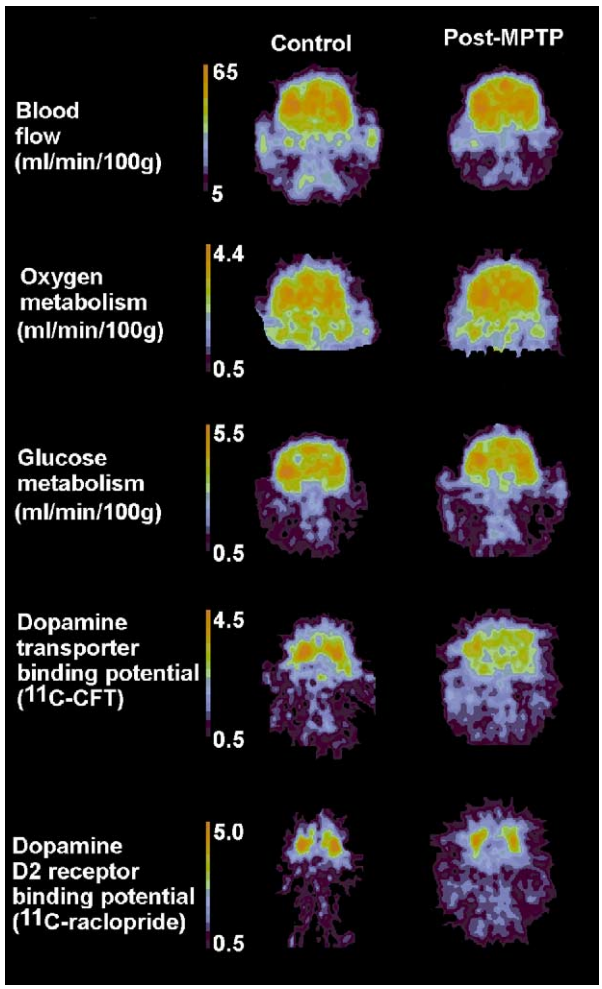

Fig. 5. Coronal midbrain slices of a monkey brain illustrate the quantitative distribution of hemodynamic, metabolic, and dopamine receptor function before and after MPTP neurotoxicity. Studies of blood flow were conducted with a steady-state inhalation technique using a $C^{15}O_2$ gas mixture (Jones, 1976). Studies of oxygen metabolism were conducted with a steady-state inhalation technique using a $^{15}O_2$ gas mixture (Jones, 1976; Subramanyam, 1978). Studies of glucose metabolism were conducted with [^{18}F]FDG (2-^{18}F-fluoro-2-deoxy-D-glucose). Studies of dopamine transporters were conducted with [^{11}C]CFT (2β-carbomethoxy-3β-(4-fluorophenyltropane). Studies of dopamine D_2 receptors were conducted with [^{11}C]raclopride.

Table 1
Radioactivity based on the volumetric data analyses compared to the measured radioactivity and the conventional 2-dimensional pixel analyses in two concentric spheres

	Inner sphere (μCi/100 ml)	Outer sphere (μCi/100 ml)
First experiment		
Radioactivity determined on the volumetric data analyses	86 +/− 7	893 +/− 62
Measured radioactivity	0	869 +/− 11
Conventional 2D ROI analyses	110 +/− 12	1012 +/− 94
Second experiment		
Radioactivity determined on the volumetric data analyses	527 +/− 20	239 +/− 7
Measured radioactivity	516 +/− 5	225 +/− 4
Conventional 2D ROI analyses	572 +/− 72	275 +/− 55

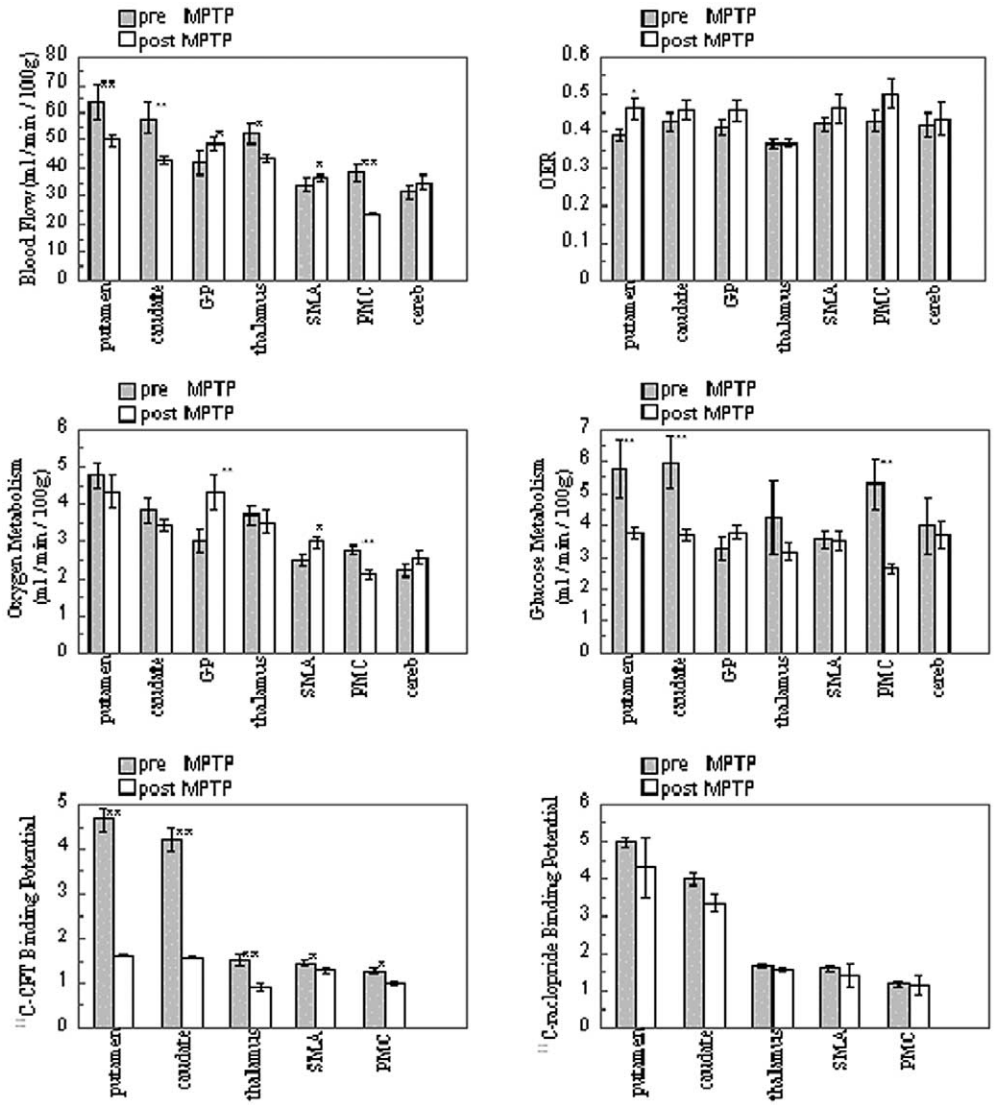

Fig. 6. Quantitative topographic distribution (mean +/− SEM) of hemodynamic, metabolic, and dopamine receptor function before and after MPTP-induced neurotoxicity in the different brain areas. All the data analyses are based on volumetric data analyses using fused PET and MR images. Significant difference was calculated as compared to the pre-MPTP values by using Dunnett's *t* test. Blood flow studies show a significant decrease in putamen, caudate, and PMC ($P < 0.01$) and thalamus ($P < 0.05$) and an increase in GP and SMA ($P < 0.05$). Oxygen extraction fraction (OER) shows an overall increase with significant change in putamen ($P < 0.05$). Oxygen metabolism shows a significant increase in the GP ($P < 0.01$) and SMA ($P < 0.05$) and a significant decrease in PMC ($P < 0.01$) and an overall decrease in the other brain areas. Glucose metabolism shows a significant decrease in putamen, caudate, and PMC ($P < 0.01$) and an overall decrease in the other brain areas but GP and SMA. Dopamine transporter binding investigated by [^{11}C]CFT shows significant decrease in putamen, caudate, and thalamus ($P < 0.01$) and SMA and PMC ($P < 0.05$). Dopamine D_2 receptor binding investigated by [^{11}C]raclopride does not show any significant changes.

Studies of oxygen extraction fraction and metabolism

After the blood flow study, the inhalation gas mixture was switched to $^{15}O_2$. In 10–12 min a steady-state activity level was obtained in the brain based on stabilized oxygen metabolism and blood flow (Jones et al., 1976; Subramanyam et al., 1978). A similar sequential imaging over the whole brain was performed as above. During imaging arterial blood was drawn to determine blood gases, hematocrite, hemoglobin, and radioactivity levels in the plasma and whole blood. These data are necessary to calculate the oxygen extraction fraction (Jones, 1976; Subramanyam et al., 1978). Regional cerebral oxygen metabolism can be calculated when blood flow, oxygen extraction fraction, blood gases, and hemoglobin are known (Subramanyam et al., 1978). Finally, values of oxygen metabolic rate were converted to molar units for stoichiometric comparisons with glucose utilization.

Studies of glucose metabolism

Studies of glucose metabolism were done using [^{18}F]FDG (2-^{18}F-fluoro-2-deoxy-D-glucose) as a tracer. FDG distributes in tissue like glucose but remains unme-

Table 2
Stoichiometry of glucose utilization and O_2 consumption in different brain areas before and after MPTP

	Before MPTP	After MPTP
Putamen	6.68 +/− 1.06	8.71 +/− 0.86
Caudate	5.13 +/− 0.69	6.92 +/− 0.34
GP	7.39 +/− 0.78	8.23 +/− 0.92
Thalamus	6.98 +/− 1.91	7.71 +/− 0.71
SMA	5.63 +/− 0.89	5.84 +/− 0.32
PMC	4.19 +/− 0.53	6.00 +/− 0.54
Cerebellum	4.42 +/− 0.98	5.04 +/− 0.38

tabolized in the form of 6-phosphate making quantitative imaging studies possible. The kinetic model of Sokoloff et al. (1977) extended by Phelps et al. (1979) was used in data analysis. Following a rapid intravenous injection of 5 mCi of ^{18}F-FDG, dynamic PET images were acquired at a level 15 mm anterior from the earbar for 30 min using an acquisition time of 15 s. After this, when activity had reached a steady-state level, coronal slices were acquired over the brain at 5-mm steps starting from the cerebellar level and an acquisition time of 60 s. Arterial blood samples were drawn for determination of plasma radioactivity. The plasma data were fitted to a 2-exponential function and used as an input function in calculating glucose metabolic rate. In addition, arterial glucose values were determined before and after the experiment. Values for the transport parameters k_1–k_4 were calculated from the dynamic tissue data using plasma input function (Phelps et al., 1979). Values for regional cerebral glucose metabolism were calculated using transport parameters and blood data information, regional tissue data from the areas of interest and a value of 0.5 for the lumped constant (Reivich et al., 1985). Finally, the values of glucose metabolic rate were converted to molar units for stoichiometric comparison with O_2 consumption.

Studies of dopamine D_2 receptors and transporters

Each study included two experiments. The first experiment was carried out with [^{11}C]raclopride to investigate dopamine D_2 receptors, and the second experiment was conducted 2–3 h later with [^{11}C]CFT (2β-carbomethoxy-3β-(4-fluorophenyltropane) in order to investigate dopamine transporters. Radiolabeled ligand, [^{11}C]raclopride (Ehrin et al., 1985) or [^{11}C]CFT (Brownell et al., 1996) (6–8 mCi, specific activity 600–1000 mCi/μmol) was injected into the femoral vein; and imaging data were acquired stepwise on seven coronal brain levels, initially using 15 s per image. The acquisition time was subsequently increased to 60 s, the total imaging time being 90 min in both experiments. Eighteen arterial blood samples of 0.1 ml were drawn at different time points starting from 10 s frequency and ending with 15 min frequency in order to monitor the decrease in radioactivity. In addition, three arterial blood samples were drawn for HPLC analyses of metabolites of the labeled ligands.

Kinetic behavior of [^{11}C]CFT was studied with a four-parameter estimation of the three-compartmental model approach. In the three-compartmental model, the first compartment is the plasma pool, the second is the exchangeable tracer pool including free and nonspecifically bound ligand in the brain, and the third compartment is a trapped tracer pool including bound ligand in the brain. The exchangeable tracer pool contains ligand but no receptors; and the third compartment includes all the receptors, partly or totally occupied by ligands. The kinetic parameters k_3 and k_4 describe the binding to and dissociation from the receptors.

The transfer coefficients k_1–k_4 were mathematically resolved using a least-square fit, Levenburg-Marquardt method. All numerical analyses were done with the optimization tool SAAM II (Foster et al., 1994). For stabilization of the k values the fitting procedure was performed using two steps. Since the cerebellum does not have specific receptor binding or is negligible, fitting was done with the cerebellar data, letting all the k values float. The ratio k_1/k_2 was then calculated. In further iterations this fixed ratio was used as a constraint and applied with a sequential quadratic programming method combined with a cost function to reach parameter optimization. Regional binding potential was calculated as a ratio of k_3/k_4 (the ratio of the transport from the exchangeable tracer pool into the bound tracer pool to the transport from the bound tracer pool back into the exchangeable tracer pool). Regional binding potentials were

Table 3
MPTP-induced changes in dopamine receptor function, hemodynamics, and metabolism in different brain areas

	Dopamine transporter	Dopamine D_2 receptor	Blood flow	Oxygen extraction	Oxygen metabolism	Glucose metabolism
Putamen	↓**	↓	↓**	↑*	↓	↓**
Caudate	↓**	↓	↓**	↑	↓	↓**
GP	—	—	↑*	↑	↑**	↑
Thalamus	↓**	↕	↓*	↕	↓	↓
SMA	↓*	↓	↑*	↑	↑*	↕
PMC	↓*	↕	↓**	↑	↓**	↓**
Cerebellum	—	—	↑	↑	↑	↓

↑ indicates an increase, ↓ indicates a decrease and ↕ indicates no change compared to the pre-MPTP value.
* signs $P < 0.05$ and ** $P < 0.01$.

calculated separately for left and right caudate, putamen, thalamus, SMA, and PMC.

Results

Accuracy of the volumetric data analyses

Development of image fusion and volumetric data analysis has been an essential part of this work. This approach is absolutely necessary to obtain reliable data from small brain regions. Fig. 2 shows coronal, transverse, and sagittal segmentation with 3-mm steps (slice thickness) of a volume-rendered MR images fused with PET images of dopamine D_2 receptor distribution after MPTP. The original PET images were acquired with 5-mm steps and a slice thickness of 5 mm. Fig. 3 demonstrates selection of the regions of interest on a single slice level.

The validation of the volumetric data analyses was done with a phantom of concentric spheres (Fig. 4). Table 1 shows the accuracy of the obtained results based on the volumetric data analyses and actual measurement of radioactivity, with comparison to the conventional 2-dimensional pixel analyses. In the first experiment radioactivity was only in the outer sphere and the calculated radioactivity using volumetric data analyses was 3% and with conventional 2D pixel analyses 16% higher that the measured radioactivity. There was only water in the inner sphere, but because of the scatter and spillover of the radioactivity in the outer sphere it was possible to record an activity, which corresponded 9.7% of the activity in the outer sphere using volumetric data analyses and 10.9% using 2D analyses.

In the second experiment radioactivity was in both spheres with the inner sphere more active. The values calculated using volumetric data analyses were 2–6 % higher than measured radioactivity while conventional 2D pixel analyses gave 11–22% higher values. The activity concentration in the inner sphere was in the same range as the striatal activity concentration in blood flow and receptor studies before MPTP toxication. These phantom studies were not corrected for the partial volume effects, because in each slice the smallest thickness of the sphere in the image was equal or bigger than two times the resolution element of the tomograph (Hoffman et al., 1979).

These basic tools have been used to analyze data for blood flow, oxygen extraction fraction, and metabolism as well as glucose metabolism and binding parameters for dopamine transporters and dopamine D_2 receptors in different brain regions.

Hemodynamics and cerebral energy metabolism

Fig. 5 (see Table 3) shows the quantitative distribution and calculated values of blood flow, oxygen metabolism, glucose metabolism, dopamine transporters, and dopamine D_2 receptors at one midbrain level before and after MPTP. From these images it can be observed, that the most striking change after MPTP is the decrease in striatal dopamine transporter binding. Fig. 6 shows the calculated values obtained by volumetric data analyses in different brain areas of hemodynamic, metabolic, and dopamine receptor function both before and after MPTP induced neurotoxicity.

The largest decrease in blood flow after MPTP was observed in the primary motor cortex (39+/−4%). Blood flow was decreased in the striatal area (caudate and putamen) by 22–26%, and in the thalamus by 17+/−3%. In the globus pallidus, blood flow was increased by 15+/−3% and in the SMA by 4+/−1%.

After MPTP, oxygen extraction fraction was moderately enhanced in other brain areas but the thalamus (Fig. 6). Values for oxygen metabolism in the GP and SMA were significantly elevated, partly being a reflection of elevated oxygen extraction fraction. Oxygen metabolism was decreased in the putamen and caudate by 10+/−2% and significantly in the PMC (23+/−2%).

Glucose metabolism was decreased in all other brain areas but the GP (Fig. 6). In the striatal area glucose utilization was decreased by 35+−/17% in the caudate, 38+/−8% in the putamen, 25+/−7% in the thalamus, and (50+/−12%) in the PMC. Glucose utilization was enhanced in the GP by 15+/−3% (see Table 3).

Stoichiometry of glucose utilization and O_2 consumption

Table 2 shows the calculated values for stoichiometric balance in different brain areas before and after MPTP. The stoichiometric balance increased in all brain areas after MPTP, indicating that, in addition to glucose, other substrates were also metabolized after MPTP.

Dopamine transporters and receptors

The binding of [^{11}C]CFT was significantly decreased in the putamen (65+/−4%), caudate (62+/−5%), thalamus (39+/−4%), SMA (25+/−2%), and PMC (25+/−2%) (Figs. 5 and 6), indicating degeneration of the dopamine transporter sites in the presynaptic terminals. [^{11}C] Raclopride binding in dopamine D_2 receptors showed overall decreases (Figs. 5 and 6, Table 3). However, because of a large variation in the results there was no significant change in raclopride binding after MPTP.

Studies of receptor function and metabolism in relation to neural circuitry

To compare the obtained experimental results of dopamine receptor function, hemodynamics, and metabolism with the known neural circuitry, we analyzed MPTP neurotoxicity-induced changes in different brain areas, conventionally included in neurophysiological studies of the neural networks. Table 3 shows the direction of MPTP-induced significant changes in different brain areas.

Discussion

Parkinson's disease is characterized neuropathologically by a severe depletion of dopamine neurons in the basal ganglia. Our experiments, conducted in primates after MPTP-induced neurotoxicity, showed significantly decreased binding of [^{11}C] CFT in striatum, indicating depletion of presynaptic dopamine terminals. We have published this observation in 1992 (Hantraye et al., 1992), and in 1994 we further demonstrated the correlation to locomotor activity (Wullner et al., 1994). In these experiments we also found that the total dose or injection period of MPTP does not correlate with locomotor activity or clinical scores (Wullner et al., 1994). Since then, about 200 papers have been published, with a unanimous observation of declining dopamine transporter binding (van Dyck et al., 2002; Antonini et al., 2001; Chouker et al., 2001; Huang et al., 2001; Marck et al., 2001; Sakakibara et al., 2001). Even though there is an unequivocal decline in presynaptic dopamine transporter binding in PD, there is inconsistency in reported results of [^{11}C]raclopride binding in dopamine D_2 receptors in PD (Doudet et al., 2000; Hwang et al., 2002; Kaasinen et al., 2000). In our present experiments, we have found a tendency for a decrease but with a large variation in dopamine D_2 receptor binding after MPTP toxication. During MPTP administration (acute MPTP-induced neurotoxicity) and after 6-hydroxydopamine toxicity (van Nguyen et al., 2000) we have observed a moderately increased [^{11}C]raclopride binding in D_2 receptors. Altogether, our observations of dopamine D_2 receptor binding are consistent with a number of publications that propose a biphasic behavior of D_2 receptor binding; indicating that in the early phase of Parkinson's disease, D_2 receptor binding is enhanced because of supersensitivity and it will decline later with progression of the disease (Stoessl and de la Fuentes-Fernandez, 2003; Hwang et al., 2002; Kaasinen et al., 2000). In addition, there are some other aspects, which might effect on [^{11}C]raclopride binding. First, it has low binding affinity, and it is impossible to determine whether the changes in binding reflect alterations in the number of available dopamine receptors or whether they are due to changes in synaptic dopamine concentration (Stoessl and de la Fuente-Fernandez, 2003). In addition, it may be possible that these effects could cancel each other out.

By using the volume of interest determined from the fusion with MR images we were able to investigate also binding characteristics of [^{11}C]CFT and [^{11}C]raclopride in the thalamus, SMA, and PMC. Using conventional PET image analysis it is impossible to localize these sites because the accumulation of radioactivity is so low compared to striatal accumulation. The binding values obtained (Figs. 5 and 6) correlate well with the values obtained using autoradiographic techniques (Kaufman and Madras, 1992).

In addition to studies of dopamine transporters and dopamine D_2 receptors, we conducted hemodynamic and metabolic studies in this preclinical model of PD with the ultimate aim of finding parallels to human PD in adaptive changes including metabolic neural networks and dopaminergic function.

Brooks (1997, 1999) has shown that slowness in free performed motion in PD patients corresponds with changes in blood flow in the supplementary motor area and dorsal prefrontal cortex, areas which get subcortical input from the basal ganglia. Notably, blood flow changes consistent with a compensatory overactivation in premotor area were observed. In PD, there appears to be a synchronization of GPe and GPi output signals as a result of the loss of DA tonic input to the putamen; that together with a reduced thalamic input to the SMA and PM cortices may explain the motor signs of PD (Brooks, 1999; Eidelberg et al., 1995b; Schmidt and Ferger, 2001). Moreover, the recruitment of more cortical regions and the increased and widespread activation of PM and SMA-associated cortices suggest that these structures are compensating for the abnormal input, to be able to activate the motor cortex for initiation of the movement (Brooks, 1997; Eidelberg et al., 1996).

We observed enhanced blood flow in the supplementary motor area as well as in the globus pallidus, while blood flow was decreased in the putamen, caudate, and primary motor cortex of the parkinsonian primate. Oxygen metabolism was marginally enhanced in the globus pallidus and supplementary motor area and decreased in the putamen, caudate, and primary motor cortex. Glucose metabolism was decreased in all brain areas after MPTP but the GP and SMA. In short, we found (1) a decreased striatal dopamine transporter binding, indicating degeneration of presynaptic terminals; (2) an increased blood flow in the globus pallidus, indicating activation in that brain area; (3) a decreased glucose metabolism in the thalamus, indicating decreased energy metabolism; and (4) decreased blood flow and glucose metabolism in the PMC, indicating decreased motor activity. However, at the same time, blood flow in the SMA was increased while no change in glucose metabolism was observed indicating a compensatory mechanism in motor function. These observations (see Table 3) support a neural circuitry-based reasoning for changes seen in functional interactions of the motor system in human parkinsonism (Wichman and DeLong, 2003; Carbon et al., 2003; DeLong and Wichman, 2001; Isacson et al., 2001).

As a comparison of the values obtained for the regional changes of glucose utilization in this "chronic" MPTP model it can be emphasized that Palombo et al. (1991) obtained 40% enhanced glucose utilization in a globus pallidus by autoradiographic studies of [^{14}C]deoxyglucose in a hemiparkinsonian model induced by a unilateral intracarotid administration of MPTP into the striatum. As well Porrino et al. (1987) found a significantly reduced glucose utilization in substantia nigra, thalamus, and ventral tegmental area and increased values in globus pallidus by autoradiographic studies of [^{14}C]deoxyglucose in MPTP-treated awake primates. Eidelberg et al. (1994) found in human Parkinson's disease patients a 20–30% average decrease in

glucose utilization depending on the level of disease. It is obvious that there is a difference in absolute values between animal models and species. However, interestingly the trend of the changes is similar.

We have considered the globus pallidus as one brain region in these experiments. However, it has two parts interna and externa, which have different functions. The observed increase in hemodynamic functions, blood flow and oxygen and glucose metabolism, in the GP area could reflect (1) an increased firing of GPi neurons (which project to the thalamus), (2) an increased metabolism at synaptic terminals from GPe and putamen, projecting to GPi, or (3) a metabolic activity of interneurons of GP. Differentiation of these mechanisms is not possible with the conducted PET techniques, but requires additional electrophysiological measurements.

In the normal in vivo state, glucose is the only substrate for energy metabolism in the brain. Under normal circumstances, no other potential energy yielding substrate has been found to be extracted from the blood in more than trivial amounts. For complete oxidation of glucose, the theoretical ratio of O_2 to glucose utilization is 6.0. A value of 5.2 has been obtained in human studies conducted with $^{15}O_2$ gas and [^{18}F]FDG (Frey, 1999). In the present experiments, an average value for the stoichiometry of the glucose utilization and oxygen consumption is 5.8+/− 0.6 before MPTP regimen and 7.0+/−0.9 after MPTP calculated as a mean of 8 investigated brain areas (see Table 2). An average 20% increase in oxygen consumption compared to glucose utilization after MPTP may be explained by a reduced mitochondrial function or combined effect of decreased metabolism and anesthesia. Halothane anesthesia might have an enhancing effect on the absolute values of blood flow and metabolism depending on the level of halothane concentration. The effect is, however, smaller in the spontaneous inhalation used in these experiments (Amory et al., 1971). In addition, the same anesthesia protocol was used before and after MPTP so the possible anesthesia-induced changes were minimized in the evaluation of MPTP-induced changes on blood flow, metabolism, and dopaminergic function.

To obtain quantitative information from small brain areas in imaging studies, we have developed a volumetric technique for data analyses and used fused PET and MRI data. In addition, the primate brain atlas was utilized to outline the regions of interest on MR images. Even when the selection of the volume of interest is accurate on a technical level, there is a potential error in the absolute values because of effects of partial volume (Hoffman et al., 1979). In addition, outlining tiny brain areas there is a personal factor. When these data were analyzed by two scientists independently, there was an average of 20% difference between the absolute values, they obtained. However, when they analyzed the data together, the values were equal to the lower values in the first time. Moreover, in the absolute values internal scatter radiation is a factor in nearby low activity tissue if the neighboring tissue has a high activity concentration. In biological studies this shows up especially in the [^{11}C]CFT studies of dopamine transporters, where the putamen has a high activity accumulation compared to the nearby tissues (Fig. 5). To validate volumetric data analyses, imaging studies in concentric sphere phantoms were conducted. The absolute values calculated for radioactivity concentration were higher than measured radioactivity mainly because of the internal scatter. This is clearly demonstrated in the first phantom study when the inner sphere did not have any radioactivity but based on data acquisition and analyses it had about 10% of the activity of the outer sphere (Table 1).

These experiments provide in-depth information on changes in metabolic and dopaminergic function in neural networks after MPTP-induced parkinsonism in primates. This information is valuable for investigations of a compensatory mechanism during degeneration and structural repair. In addition, these experiments enhance the use of MPTP neurotoxicity as a model to investigate human Parkinson's disease.

Acknowledgments

We thank cyclotron operators William Bucklewicz and David Lee for preparing radiopharmaceuticals for these experiments as well as Jack McDowell for taking good care of the primates. This work was supported by DOD Grant DAMD17-98-1-8618 and NINDS Grant NS P50-39793 to O.I. at McLean Hospital and DOD Grant DAMD17-99-1-9555 to A.-L.B. at Massachusetts General Hospital. F.C. was supported by the Medical Research Council of Canada.

References

Alexander, G., 1987. Selective neuronal discharge in monkey putamen reflects intended direction of planned limb movement. Exp. Brain Res. 67, 623–634.

Alexander, G., DeLong, M.R., Strick, P.L., 1986. Parallel organization of functionally segregated circuits linking basal ganglia and cortex. Annu. Rev. Neurosci. 9, 357–381.

Alexander, G.E., Crutcher, M.D., Delong, M.R., 1990. Basal ganglia thalamo-cortical circuits: parallel substrates for motor, oculomotor, "prefrontal" and "limbic" functions. Prog. Brain Res. 85, 119–146.

Amory, D.W., Steffenson, J.L., Forsyth, R.P., 1971. Systemic and regional blood flow changes during halothane anesthesia in the Rhesus monkey. Anesthesiology 35, 81–90.

Antonini, A., Kazumata, K., Feigin, A., Mandel, F., Dhawan, V., Margouleff, C., et al., 1998. Differential diagnosis of parkinsonism with [^{18}F]fluorodeoxyglucose and PET. Mov. Disord. 13, 268–274.

Antonini, A., Moresco, R.M., Gobbo, C., De Notaris, R., Panzacchi, A., Barone, P., et al., 2001. The status of dopamine nerve terminals in Parkinson's disease and essential tremor: a PET study with the tracer [^{11}C]FE-CIT. Neurol. Sci. 22, 47–48.

Antonini, A., Vontobel, P., Psylla, M., Gunther, I., Maguire, P.R., Missimer, J., et al., 1995. Complementary positron emission tomographic studies of the striatal dopaminergic system in Parkinson's disease. Arch. Neurol. 52, 1183–1190.

Berding, G., Odin, P., Brooks, D.J., Nikkhah, G., Matthies, C., Peschel, T., et al., 2001. Resting regional cerebral glucose metabolism in advanced Parkinson's disease studied in the off and on conditions with [^{18}F]FDG-PET. Mov. Disord. 16, 1014–1022.

Bohnen, N., Minoshima, S., Giordani, B., Frey, K.A., Kuhl, D.E., 1999. Motor correlates of occipital glucose hypometabolism in Parkinson's disease without dementia. Neurology 52, 541–546.

Brooks, D., 1997. PET and SPECT studies in Parkinson's disease. Baillieres Clin. Neurol. 6, 69–87.

Brooks, D., 1999. Functional imaging of Parkinson's disease: is it possible to detect brain areas for specific symptoms? J. Neural. Transm. Suppl. 56, 139–153.

Brooks, D.J., 2001. Cerebral blood flow activation studies, in: Calne, D., Calne, S. (Eds.), Parkinson's Disease: Advances in Neurology, Vol. 86. Lippincott Williams & Wilkins, Philadelphia, pp. 225–235.

Brownell, A.-L., Elmaleh, D.E., Meltzer, P.C., Shoup, T.M., Brownell, G.L., Fischman, A.J., et al., 1996. Cocaine congeners as PET imaging probes for dopamine terminals. J. Nucl. Med. 37, 1186–1192.

Brownell, A.-L., Jenkins, B.G., Elmaleh, D.R., Deacon, T.W., Spealman, R.D., Isacson, O., 1998. Combined PET/MRS brain studies show dynamic and long-term physiological changes in a primate model of Parkinson disease. Nature Med. 4, 1308–1312.

Brownell, A.-L., Jenkins, B.G., Isacson, O., 1999. Dopamine imaging markers and predictive mathematical models for progressive degeneration in Parkinson's disease. Biomed. Pharmacother. 53, 131–140.

Brownell, G.L., Burnham, C.A., Stearns, C.W., Chesler, D.A., Brownell, A.-L., Palmer, M., 1989. Development in high-resolution positron emission tomography at MGH. Int. J. Imaging Systems Technol. 1, 207–217.

Carbon, M., Edwards, C., Eidelberg, D., 2003. Functional brain imaging in Parkinson's disease, in: Gordin, A., Kaakkola, S., Teravainen, H. (Eds.), Parkinson's Disease: Advances in Neurology, vol. 91. Lippincott Williams & Wilkins, Philadelphia, pp. 175–181.

Checkoway, H., Nelson, L.M., 1999. Epidemiologic approaches to the study of Parkinson's disease etiology. Epidemiology 10, 327–336.

Chesler, D., 1973. Positron tomography and three-dimensional reconstruction technique, in: Freedman, G.S. (Ed.), Tomographic Imaging in Nuclear Medicine. Soc. Nucl. Med., New York, pp. 176–183.

Chouker, M., Tatsch, K., Linke, R., Pogarell, O., Hahn, K., Schwarz, J., 2001. Striatal dopamine transporter binding in early to moderately advanced Parkinson's disease: monitoring of disease progression over 2 years. Nucl. Med. Commun. 22, 721–725.

Crutcher, M., DeLong, M.R., 1984. Single cell studies of the primate putamen. II. Relations to direction of movement and pattern of muscular activity. Exp. Brain Res. 53, 244–258.

DeLong, M., Wichman, T., 2001. Deep brain stimulation for Parkinson's disease. Ann. Neurol. 49, 142–143.

Doudet, D.J., Holden, J.E., Jivan, S., McGeer, E., Wyatt, R.J., 2000. In vivo PET studies of the dopamine D2 receptors in rhesus monkeys with long term MPTP-induced parkinsonism. Synapse 38, 105–113.

Eberling, J., Richardson, B.C., Reed, B.R., Wolfe, N., Jagust, W.J., 1994. Cortical glucose metabolism in Parkinson's disease without dementia. Neurobiol. Aging 15, 329–335.

Ehrin, E., Farde, L., de Paulis, T., Eriksson, L., Greitz, T., Johnstrom, P., et al., 1985. Preparation of ^{11}C-labelled raclopride, a new potent dopamine receptor antagonist: preliminary PET studies of cerebral dopamine receptors in the monkey. Int. J. Appl. Radiat. Isot. 36, 269–273.

Eidelberg, D., Moeller, J.R., Dhawan, V., Spetsieris, P., Takikawa, S., Ishikawa, T., et al., 1994. The metabolic topography of parkinsonism. J. Cereb. Blood Flow Metab. 14, 783–801.

Eidelberg, D., Moeller, J.R., Ishikawa, T., Dhawan, V., Spetsieres, P., Chaly, T., et al., 1995a. Assessment of disease severity in parkinsonism with fluorine-18-fluorodeoxyglucose and PET. J. Nucl. Med. 36, 378–383.

Eidelberg, D., Moeller, J.R., Ishikawa, T., Dhawan, V., Spetsieres, P., Chaly, T., et al., 1995b. Early differential diagnosis of Parkinson's disease with 18F-fluorodeoxyglucose and positron emission tomography. Neurology 45, 1995–2004.

Eidelberg, D., Moeller, J.R., Ishikawa, T., Dhawan, V., Spetsieres, P., Silbersweig, D., et al., 1996. Regional metabolic correlates of surgical outcome following unilateral pallidotomy for Parkinson's disease. Ann. Neurol. 39, 452–459.

Foster, D., Barrett, P.H.R., Bell, B.M., Beltz, W.F., Cibelli, C., Golde. H.1994. Simulation, analysis and modeling software. BMES Bull., 18.

Frackowiak, R., Lenzi, G.L., Jones, T., Heather, J.D., 1980. Quantitative measurement of regional cerebral blood flow and oxygen metabolism in man using 15O and positron emission tomography: theory, procedure and normal values. J. Comput. Assist. Tomogr. 4, 727–736.

Frey, K.A., 1999. Positron emission tomography, in: Siegel, G.J., Agranoff, B.W., Albers, R.W., Fisher, S.K., Uhler, M.D. (Eds.), Basic neurochemistry. Lippincott-Raven, Philadelphia, pp. 1109–1131.

Fukuda, M., Mentis, M.J., Ma, Y., Dhawan, V., Antonini, A., Lang, A.E., et al., 2001. Networks mediating the clinical effects of pallidal brain stimulation for Parkinson's disease. A PET study of resting-state glucose metabolism. Brain 124, 1601–1609.

Gorrell, J., DiMonte, D., Graham, D., 1996. The role of environment in Parkinson's disease. Environ. Health Perspect. 104, 652–654.

Hantraye, P., Brownell, A.-L., Elmaleh, D.R., Spealman, R.D., Wullner, U., Brownell, G.L., et al., 1992. Dopamine fiber detection by [11C]-CFT and PET in a primate model of parkinsonism. NeuroReport 3, 265–268.

Hoffman, E.J., Huang, S.C., Phelps, M.E., 1979. Quantitation in positron emission tomography. 1 Effect of object size. J. Comput. Assist. Tomogr. 3, 299–308.

Huang, H.S., Lin, C.Z., Lin, J.C., Wey, S.P., Ting, G., Liu, R.S., 2001. Evaluation of early-stage Parkinson's disease with 99mTc-TRODAT-1 imaging. J. Nucl. Med. 42, 1303–1308.

Hwang, W.J., Yao, W.J., Wey, S.P., Shen, L.H., Ting, G., 2002. Down-regulation of striatal dopamine D2 receptors in advanced Parkinson's disease contributes to the development of motor flunctuation. Eur. Neurol. 47, 113–117.

Imon, Y., Matsuda, H., Ogawa, M., Kogure, D., Sunohara, N., 1999. SPECT image analysis using statistical parametric mapping in patients with Parkinson's disease. J. Nucl. Med. 40, 1583–1589.

Isacson, O., van Horne, C., Schumacher, J.M., Brownell, A.-L., 2001. Improved surgical cell therapy in Parkinson's disease—physiological basis and new transplantation methodology, in: Calne, D., Calne, S. (Eds.), Parkinson's Disease: Advances in Neurology, Vol. 86. Lippincott Williams & Wilkins, Philadelphia, pp. 447–454.

Jones, T., Chesler, D.A., Ter-Pogossian, M.M., 1976. The continuous inhalation ofxygen-15 for assessing regional oxygen extraction fraction in the brain of man. Br. J. Radiol. 49, 339–343.

Kaasinen, V., Ruottinen, H.M., Nagren, K., Lehikoinen, P., Oikonen, V., Rinne, J.O., 2000. Upregulation of putaminal D2 receptors in early Parkinson's disease: a comparative PET study with [^{11}C]raclopride and [^{11}C]N-methylspiperoni. J. Nucl. Med. 41, 65–70.

Kaufman, M.J., Madras, B.K., 1992. Distribution of cocaine recognition sites in monkey brain. II.Ex vivo autoradiography with [^{3}H]CFT and [^{125}I]RTI-55. Synapse 12, 99–111.

Kish, S., Shannak, K., Hornykiewicz, O., 1988. Uneven pattern of dopamine loss in the striatum of patients with idiopathic Parkinson's disease. N. Engl. J. Med. 318, 876–880.

Marck, K., Innis, R., van Dyck, C., Fussel, B., Early, M., Eberly, S., et al., 2001. [^{123}I]Beta-CIT SPECT imaging assessment of the rate of Parkinson's disease progression. Neurology 57, 2089–2094.

Markus, H., Lees, A.J., Lennox, G., Marsden, C.D., Costa, D.C., 1995. Patterns of regional cerebral blood flow in corticobasal degeneration studied using HMPAO SPECT; comparison with Parkinson's disease and normal controls. Mov. Disord. 10, 179–187.

Marsden, C.D., 1992. Parkinson disease. Postgrad. Med. J. 68, 538–543.

Mizuno, Y., Shimoda-Matsubayashi, S., Matsumine, H., Morikawa, N., Hattori, N., Kondo, T., 1999. Genetic and environmental factors in the pathogenesis of Parkinson's disease. Adv. Neurol. 80, 171–179.

Moeller, J.R., Eidelberg, D., 1997. Divergent expression of regional metabolic topographies in Parkinson's disease and normal aging. Brain 120, 2197–2206.

Palombo, E., Porrino, L.J., Bankiewicz, K.S., Crane, A.M., Sokoloff, L., Kopin, I.J., 1990. Local cerebral glucose utilization in monkeys with hemiparkinsonism induced by intracarotid infusion of the neurotoxin MPTP. J. Neurosci. 10, 860–869.

Palombo, E., Porrino, L.J., Crane, A.M., Bankiewicz, K.S., Kopin, I.J., Sokoloff, L., 1991. Cerebral metabolic effects of monoamine oxidase in normal and 1-methyl-4-phenyl-1,2,3,6-tetrahydropyridine acutely treated monkeys. J. Neurochem. 56, 1639–1646.

Paxinos, G., Huang, X.-F., Toga, A.W., 2000. The Rhesus Monkey Brain Atlas in Stereotaxic Coordinates. Academic Press, San Diego.

Phelps, M.E., Huang, S.C., Hoffman, E.J., Selin, C., Sokoloff, L., Kuhl, D., 1979. Tomographic measurement of local cerebral glucose metabolic rate in humans with (F-18-2-fluoro-2- deoxy-D-glucose: validation of method. Ann. Neurol. 6, 371–388.

Porrino, L., Burns, R.S., Crane, A.M., Palombo, E., Kopin, I.J., Sokoloff, L., 1987. Changes in local cerebral glucose utilization associated with Parkinson's syndrome induced by 1-methyl-4-phenyl-1,2,3,6-tetrahydropyridine (MPTP) in the primate. Life Sci. 40, 17657–17664.

Puyau, M., Adolph, A.L., Vohra, F.A., Butte, N.F., 2002. Validation and calibration of physical activity monitors in children. Obes. Res. 10, 150–157.

Reivich, M., Alavi, A., Wolf, A., Fowler, J., Russell, J., Arnett, C., et al., 1985. Glucose metabolism rate kinetic model parameter determination in humans: the lumped constants and rate constants for [^{18}F]fluorodeoxy- and [^{11}C]deoxyglucose. J. Cereb. Blood Flow Metab. 5, 179–192.

Sakakibara, R., Shinotoh, H., Yoshiyama, M., Hattori, T., Yamanishi, T., 2001. SPECT imaging of the dopamine transporter with [^{123}I]-beta-CIT reveals marked decline of nigrostriatal dopaminergic function in Parkinson's disease with urinary dysfunction. J. Neurol. Sci. 187, 55–59.

Schapira, A.H.V., 1996. Neurotoxicity and the mechanisms of cell death in Parkinson's disease, in: Battistin, L., Scarlato, G., Carceni, T., Ruggieri, S. (Eds.), Advances in Neurology, Vol. 69. Lippincott-Raven, Philadelphia, pp. 161–165.

Schmidt, N., Ferger, B., 2001. Neurochemical findings in the MPTP model of Parkinson's disease. J. Neural. Transm. 108, 1263–1282.

Sokoloff, L., Reivich, M., Kennedy, C., Des Rosiers, M.H., Patlak, C.S., Pettigrew, K.D., et al., 1977. The (C-14) deoxy glucose method for the measurement of local cerebral glucose utilization: theory, procedure, the normal values in the conscious and anesthetized albino rat. Neurochemistry 28, 897–916.

Stoessl, A.J., de la Fuente-Fernandez, R., 2003. Dopamine receptor in Parkinson's disease: imaging studies, in: Gordin, A., Kaakkola, S., Teravainen, H. (Eds.), Parkinson's Disease: Advances in Neurology, Vol. 91. Lippincott-Raven, Philadelphia, pp. 65–71.

Subramanyam, R., Alpert, N.M., Hoop Jr., B., Brownell, G.L., Taveras, J.M., 1978. A model for regional cerebral oxygen distribution during continuous inhalation of 15O2, C15O, and C15O2. J. Nucl. Med. 19, 43–53.

van Dyck, C., Seibyl, J.P., Malison, R.T., Laruelle, M., Zoghbi, S.S., Baldwin, R.M., et al., 2002. Age-related decline in dopamine transporters: analysis of striatal subregions, nonlinear effects, and hemispheric asymmetries. Am. J. Geriatr. Psychiatry 10, 36–43.

van Nguyen, T., Brownell, A.-L., Chen, Y.I., Livni, E., Coyle, J.T., Rosen, B.R., et al., 2000. Detection of the effects of dopamine receptor supersensitivity using pharmacological MRI and correlation with PET. Synapse 36, 57–65.

Wichman, T., DeLong, M.R., 1996. Functional and pathophysiological models of the basal ganglia [Review]. Curr. Opin. Neurobiol. 6, 751–758.

Wichman, T., DeLong, M.R., 2003. Functional neuroanatomy of the basal ganglia in Parkinson's disease, in: Gordon, A., Kaakkola, S., Teravainen, H. (Eds.), Parkinson's Disease: Advances in Neurology, Vol. 91. Lippincott Williams & Wilkins, Philadelphia, pp. 9–18.

Wullner, U., Pakzaban, P., Brownell, A.-L., Hantraye, P., Burns, L., Shoup, T., et al., 1994. Dopamine terminal loss and onset of motor symptoms in MPTP-treated monkeys: a positron emission tomography study with ^{11}C-CFT. Exp. Neurol. 126, 305–309.